Dynamical windows for real-time evolution with matrix product states

Ho N. Phien,[1] Guifré Vidal,[2] and Ian P. McCulloch[1]

[1]*Centre for Engineered Quantum Systems, School of Mathematics and Physics, University of Queensland, Brisbane 4072, Australia*

[2]*Perimeter Institute for Theoretical Physics, Waterloo, Ontario, Canada N2L 2Y5*

(Received 18 December 2012; published 3 July 2013)

We propose the use of a dynamical window to investigate the real-time evolution of quantum many-body systems in a one-dimensional lattice. In a recent paper [Phien *et al.*, Phys. Rev. B **86**, 245107 (2012)], we introduced *infinite boundary conditions* in order to investigate real-time evolution of an infinite system under a local perturbation. This was accomplished by restricting the update of the tensors in the matrix product state to a finite region known as a *window*, with left and right boundaries held at fixed positions. Here we consider instead the use of a dynamical window, where the positions of left and right boundaries are allowed to change in time. In this way, all computational efforts can be devoted to the space-time region of interest, which leads to a remarkable reduction in simulation costs. For illustrative purposes, we consider two applications in the context of the spin-1 antiferromagnetic Heisenberg model in an infinite spin chain: one is an expanding window, with boundaries that are adjusted to capture the expansion in time of a local perturbation of the system; the other is a moving window of fixed size, where the position of the window follows the front of a propagating wave.

DOI: 10.1103/PhysRevB.88.035103 PACS number(s): 03.67.−a, 03.65.Ud, 02.70.−c, 05.30.Fk

I. INTRODUCTION

Ever since the density-matrix renormalization group method (DMRG) was invented in 1992 by White [1,2], it has opened new trends for the numerical study of strong correlation effects in one-dimensional quantum systems. By now, it is well established as a powerful method in producing exact results for ground state wave functions and expectation values of one-dimensional (1D) quantum systems. In addition, DMRG is not constrained to investigating static properties, but it has been extended to study dynamical properties[3–6] as well as quantum systems at finite temperature.[7,8]

The connection was not immediately made that the wave function produced by DMRG can be realized as a variational calculation in the space of matrix product states (MPS).[9–11] As it is easier, people usually prefer to implement the DMRG in terms of MPS. Furthermore, together with MPS, tensor network states have been attracting much interest from computational physicists. Algorithms have been developed based on MPS to simulate both the static and dynamical properties of 1D quantum systems. One of the most successful algorithms in MPS formalism is the time-evolving block decimation (TEBD) algorithm,[12,13] which has an equivalent DMRG formulation.[14,15] This algorithm can be used for ground state calculations, although it is not as efficient as variational minimization algorithms such as DMRG. However TEBD comes into its own for real-time evolution. More recently, a new algorithm, called the time-dependent variational principle (TDVP),[16,17] has also been introduced to study both the real- and imaginary-time dynamics for infinite one-dimensional quantum lattices.

There are many interesting problems that involve the dynamics of a small section embedded in an infinite lattice. For example, consider the real-time evolution of an infinite quantum spin chain, initially in the ground state, after one site in the middle of the chain has been locally perturbed by some spin excitation, e.g., a local S^+ operator. Before applying S^+, the state is translationally invariant and can be represented by an infinite MPS (iMPS). After applying S^+, the ground state becomes a superposition of excited states. Therefore, the iMPS can no longer be represented in a translationally invariant form. This is a huge hurdle to investigate real-time evolution of the system in the thermodynamic limit, as in principle one must use an infinite set of different tensors in the iMPS to describe the wave function of the state. This makes the simulation an impossible task. However, because the perturbation is local, one can avoid this difficulty and can still understand the dynamical properties of a system in a thermodynamic limit, as long as the range of effect is finite (or approximately so). The conventional way to solve this problem is to choose a finite lattice that is large enough that the boundaries have a minimal effect on the calculation.[14,18] As the wave function evolves in time, this local perturbation represented by a wave packet will spread throughout the system at the group velocity (for ballistic transport) or slowly spread out through the system (in the diffusive case). The system therefore needs to be large enough that the perturbation can evolve for the required time without reaching the boundary. In practice the size will need to be even larger, because the open boundary conditions, used for technical reasons in finite system calculations, give rise to Friedel oscillations that will affect the wave function even well away from the boundary.

Recently, there have been other novel algorithms that can allow to directly study the dynamics of the nontranslationally invariant systems in the thermodynamic limit while avoiding the finite-size effects. For instance, the light cone renormalization group (LCRG)[19] employs the Lieb-Robinson bound[20] to effectively evolve only a finite region (a light cone) of the lattice. Although this algorithm can be employed to investigate the dynamics of the infinite system without relying on translational invariance in using MPS, it is not efficient for a long-time evolution as the size of the light cone increases very quickly. Another technique, proposed by Bañuls *et al.*,[21] focuses on the method of contracting tensor network during the time evolution. More specifically, by folding the network in the time direction before contracting it transversely, this new technique can be used to study the dynamics of infinite systems

with local or global quenches. This method can achieve a longer-time evolution than competing techniques, however, it is quite difficult to apply when the initial state is not a product state.

Alternatively, in our previous paper,[22] we have proposed a method to study the time evolution of the system in the thermodynamic limit. We have shown that the computational cost can be substantially improved by using a much smaller finite system with *infinite boundary conditions* (IBCs). This has two advantages. First, there is no hard boundary in the system, so there are no Friedel oscillations, and away from the perturbation the system is asymptotically translationally invariant. Second, since the "boundaries" of the finite system represent an effective semi-infinite chain rather than a hard wall, there is no problem in allowing the perturbation to propagate beyond the finite region as long as the wave function does not move too far outside the effective Hilbert space of the semi-infinite chain. These are great advantages over traditional finite-size calculations. To achieve this, we divide the whole spin chain into three parts where the middle part, the so-called *window*, usually contains the perturbation, and the other two parts, on the left and right of the window, are not affected by the perturbation. The boundaries of the window are represented by an effective Hilbert space for the wave function on a semi-infinite chain.

In this paper, we further improve the computational efficiency of the IBC technique by focusing on how the wave front propagates in time. Higher efficiencies can be obtained by introducing dynamical window techniques, namely, expanding and moving the window throughout the calculation. Specifically, we will keep track of the wave front and decide to expand or move the window such that the physically relevant section of the system is well represented. An important point is that in our scheme the section of the system outside of the window, represented by an effective Hilbert space, can evolve as well so that the window size can be quite small, containing only the region of interest, without affecting the accuracy too much. Numerical results are presented for the time evolution of a local perturbation in the spin-1 antiferromagnetic (AFM) Heisenberg model.

II. INFINITE BOUNDARY CONDITIONS AND EFFECTIVE HAMILTONIAN

Before introducing the dynamical window techniques, it is important to review the definition of IBC and the effective Hamiltonian calculation. In the following, we summarize these definitions. For more detail one can refer to our previous paper.[22]

A. Infinite boundary conditions

Let us consider an infinite spin chain where the ground state is represented by an infinite translationally invariant matrix product state,

$$|\Psi\rangle = \sum_{\{s_i\}} \cdots \lambda \Gamma^{s_i} \lambda \Gamma^{s_{i+1}} \cdots |\mathbf{s}\rangle, \tag{1}$$

where $|\mathbf{s}\rangle = |\ldots \mathbf{s}_i, \mathbf{s}_{i+1}, \ldots\rangle$ is the orthonormal basis of Hilbert space $\mathcal{H} \in \mathbb{C}_d^{\otimes\infty}$ of the system (d is the dimension of local Hilbert space at each lattice site). Here we assume for simplicity that the iMPS is translationally invariant with a one-site unit cell and therefore can be represented by a tensor Γ of rank three and a diagonal matrix λ. This iMPS can be always written in the mixed canonical form as follows:

$$|\Psi\rangle = \sum_{s} \cdots A^{s_{i-1}} A^{s_i} \lambda B^{s_{i+1}} B^{s_{i+2}} \cdots |\mathbf{s}\rangle, \tag{2}$$

where tensors $A = \lambda\Gamma$ and $B = \Gamma\lambda$ satisfy the canonical form constraints

$$\sum_{s_i} A^{s_i\,\dagger} A^{s_i} = \sum_{s_i} \Gamma^{s_i\,\dagger} \rho^R \Gamma^{s_i} = \mathbb{I}, \tag{3}$$

$$\sum_{s_i} B^{s_i} B^{s_i\,\dagger} = \sum_{s_i} \Gamma^{s_i} \rho^L \Gamma^{s_i\,\dagger} = \mathbb{I}, \tag{4}$$

$\mathbb{I}$ is the identity matrix, and ρ^L and ρ^R are the left and right reduced density matrices, respectively. Note that in this representation $\rho^L = \rho^R = \lambda^2$.

We now decompose the whole chain into three sections: the window containing N sites, in the middle of the chain, and two semi-infinite chains attached to each end of the window. By introducing two boundary sites representing left and right semi-infinite chains, the infinite system can be defined as a finite system with $N + 2$ sites. These two boundary sites are also called the *infinite boundary tensors* of the finite spin chain. Then, the state of the system Eq. (2) can be written in the finite MPS form as follows:

$$|\tilde{\Psi}\rangle = \sum_{\alpha,\{s_i\},\beta} L^\alpha A_1^{s_1} \cdots A_i^{s_i} \lambda B_{i+1}^{s_{i+1}} \cdots B_N^{s_N} R^\beta |\alpha, \tilde{\mathbf{s}}, \beta\rangle, \tag{5}$$

where $|\tilde{\mathbf{s}}\rangle = |s_1, s_2, \ldots, s_N\rangle$ is the orthonormal basis of Hilbert space of the window and $|\alpha\rangle$ and $|\beta\rangle$ are orthonormal bases of effective Hilbert spaces of the left and right boundary sites with dimension χ, respectively. Note that χ is also the bond dimension of the ground state of the system. Two boundary tensors L^α and R^β are introduced to represent the two boundary sites of the finite MPS with dimensions $1 \times \chi$ and $\chi \times 1$, respectively. In practice we do not actually need the L^α and R^β tensors as these are identity elements, $L_i^\alpha = \delta_{\alpha i}$ and $R_j^\beta = \delta_{\beta j}$. However, we include them in the MPS representation so that one can understand how the infinite boundaries are incorporated in such a way that an iMPS can be effectively represented by a finite MPS. At this point, we no longer require that the MPS is translationally invariant, and the tensors A_i and B_j may all be different, for example, to represent a state that has been locally perturbed within the window.

B. Effective Hamiltonian calculation

After decomposing the entire chain into three parts, the full Hamiltonian of the system can be written as a sum of five components as

$$H = H_L + H_{LW} + H_W + H_{WR} + H_R, \tag{6}$$

where we have denoted the terms as follows: H_L and H_R are the Hamiltonians of the left and right semi-infinite chains, respectively; H_W is the Hamiltonian of the N-site window; and finally the terms H_{LW} and H_{WR} represent the interactions between the window and the left and right semi-infinite chains,

respectively. After shrinking the representation of the infinite system to the finite system, we can introduce an effective Hamiltonian as follows:

$$\tilde{H} = \tilde{H}_L + \tilde{H}_{LW} + H_W + \tilde{H}_{WR} + \tilde{H}_R. \quad (7)$$

Similar to the expression in Eq. (6), this effective Hamiltonian also contains five components. The Hamiltonian for the window H_W remains the same. Meanwhile, the other terms change and can be distinguished by the tilde symbol. As the effective Hamiltonian depends on the value of the bond dimension χ, it can only represent the system approximately. The χ-dimensional truncated Hilbert space obviously contains the original MPS approximation of the ground state itself, however, as the system evolves in time away from this state, the state of the system outside the window is constrained to lie within this truncated space, whereas the Hilbert space within the window is free to evolve. In this sense, the moving window technique can be seen as a combination of the efficient but inaccurate method of Cazalilla and Marston[6] for time evolution within a fixed Hilbert space, and TEBD/adaptive time DMRG.

In order to obtain the effective Hamiltonian of the system, one needs to find the left and right dominant eigenvectors, denoted as $\{\vec{E}_L, \vec{E}_R\}$, of the transfer matrices defined as

$$T_L = \sum_{ss'} \langle s|W|s'\rangle A^{s'\dagger} A^s \quad (8)$$

and

$$T_R = \sum_{ss'} \langle s|W|s'\rangle B^s B^{s'\dagger}, \quad (9)$$

respectively. In the above equations, we have denoted W as the matrix product operator of the Hamiltonian. Note that these dominant eigenvectors contain the components of an effective Hamiltonian and they can be understood as the block operators in the context of the DMRG algorithm. In our previous paper,[22] we describe in detail the method to obtain the effective Hamiltonian of the spin-1 AFM Heisenberg model. One can also refer to the work of Michel and McCulloch[23] for a general method to compute the effective Hamiltonian and a wide class of related operators.

III. DYNAMICAL WINDOW TECHNIQUES

Let us consider an infinite spin chain which has undergone a local perturbation. By applying the IBC, we can use a finite MPS to represent the state of the system as in Eq. (5).

The window now contains the perturbation and is allowed to dynamically change in either its size or position to follow the wave front. Dynamically changing the size or position of the window involves two basic steps, contraction of the window and expansion of the window. We now describe the technical steps involved in each case.

A. Window expansion

Expanding the window involves incorporating more degrees of freedom into the variational wave function, and this is an operation that one will typically want to do in order to follow the propagation of a perturbation as it travels through the lattice. This is achieved by incorporating some sites from the translationally invariant semi-infinite chain into the window. The window can be expanded on the left- and the right-hand side separately. For example, in order to follow the wave front of a symmetrically expanding local perturbation, we use the scheme shown in Fig. 1 with $N = 4$. The basic operation on the MPS in Eq. (5) becomes, in the case of adding two one-site unit cells to both the left and right edges of the window,

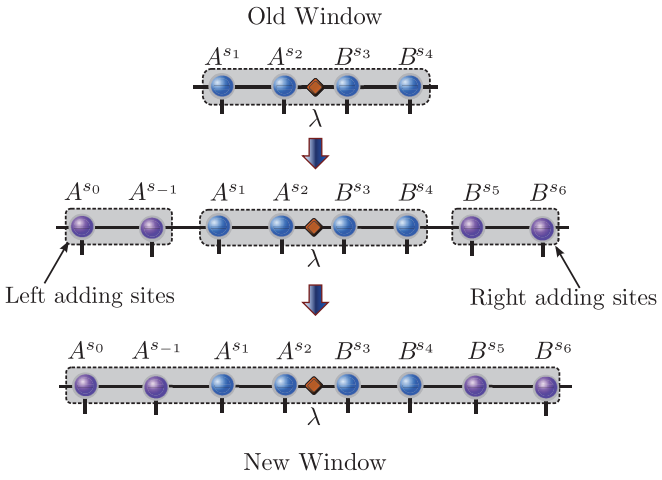

FIG. 1. (Color online) Schematic representation of window expansion technique for the $N = 4$ window. On each side of the window, there are two sites added to expand the window.

$$|\tilde{\Psi}\rangle = \sum_{\alpha,\{s_i\},\beta} L^\alpha A^{s_{-1}}_{-1} A^{s_0}_0 A^{s_1}_1 \cdots \lambda \cdots \times B^{s_N}_N B^{s_{N+1}} B^{s_{N+2}} R^\beta |\alpha, \tilde{\mathbf{s}}', \beta\rangle, \quad (10)$$

where the Hilbert space of the window is now expanded in the basis of $|\tilde{\mathbf{s}}'\rangle = |s_{-1}, s_0, s_1, s_2, \ldots, s_N, s_{N+1}, s_{N+2}\rangle$. The initial values of the left tensors $\{A_{-1}, A_0\}$ and right tensors $\{B_{N+1}, B_{N+2}\}$ are simply given by the translationally invariant matrices A and B of the ground state Eq. (2), respectively. Note that the Hilbert spaces $|\alpha\rangle$ and $|\beta\rangle$ at the left and right edges of the window are unchanged. Therefore the block operators acting on this space are also unchanged, although care needs to be taken so that the energy of the system is correctly taken into account. In calculating the effective Hamiltonian,[22] the energy per site of the infinite system appears as a separate term which is easily removed. Thus, in order to keep the total energy of the system the same constant as the window is expanded, it is convenient to subtract this energy off the Hamiltonian for the finite window as well.

B. Window contraction

The second operation that we can perform on the window is to contract the size of it, by absorbing some sites of the window into the boundary tensor. To achieve this, we contract over those sites to obtain a new set of block operators. Then, the effective Hamiltonian corresponding to the new set of block operators will now describe a semi-infinite chain plus some number of additional (not translationally invariant) sites. This procedure is implemented by following the scheme shown graphically in Fig. 2, where two sites from the window are absorbed to the boundary tensor. In particular, the right block operators after contracting two sites into the boundary tensor

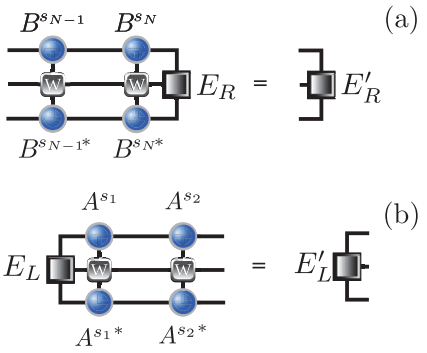

FIG. 2. (Color online) Diagrammatic illustration of how to update the block operators in the window contraction scheme. (a) The right update is performed when two sites of the window are contracted to the right boundary tensor. (b) The left update is performed when two sites of the window are contracted to the left boundary tensor.

are defined as

$$E'_R = \sum_{s_N, s_{N-1}} \langle s_N|W|s_N\rangle\langle s_{N-1}|W|s_{N-1}\rangle \times B^{s_{N-1}} B^{s_N} E_R B^{s_N\dagger} B^{s_{N-1}\dagger}, \quad (11)$$

where the tensors B^{s_N} and $B^{s_{N-1}}$ need to satisfy the right canonical form constraint in Eq. (4). Similarly, when two sites from the window are contracted to the left boundary tensor, the left block operators are determined by

$$E'_L = \sum_{s_1, s_2} \langle s_1|W|s_1\rangle\langle s_2|W|s_2\rangle \times A^{s_2\dagger} A^{s_1\dagger} E_L A^{s_1} A^{s_2}. \quad (12)$$

The tensors A^{s_1} and A^{s_2} must satisfy the left canonical form constraint in Eq. (3).

Again, one needs to take care that the total energy of the system is unchanged in this procedure, which is easily effected by subtracting a constant equal to the ground state energy per site to the Hamiltonian of the window.

C. Moving window criteria

The choice of when to move or expand the window is very important, because if the window is too large, then the calculation is less efficient, however, if the window is too small and some relevant section of the perturbation is too far outside the window, then the calculation will lose accuracy. There are many ways to formalize a criterion for when to move the window, e.g., we can look at how the wave front propagates in time and determine the maximum velocity of the excitations. However, it is much more convenient to use another criterion that relies on the change of the initial tensors L^α, A^{s_1} and the matrix λ at the edge of the window.

Let us assume that at time $t = 0$ the MPS is initially described by Eq. (5) with $i = 1$ to locate the λ matrix at the edge of the window, allowing us to define $Y_0^{\alpha,s_1} = L^\alpha A^{s_1}\lambda$ and the reduced density matrix $\rho^R = \lambda^2$. Later on, at time t the tensors A, B, λ within the window will have evolved so that we have a new $Y_t^{\alpha,s_1} = L^\alpha A'^{s_1}\lambda'$, and the reduced density matrix is also changed to $\rho^{R'} = \lambda'^2$. Note that the tensor L^α remains unchanged in time evolution from t_0 to t as the window has the same infinite boundary on its left side. We can compare the difference between Y_{t_0} and Y_t by measuring how much the reduced density matrix has changed. The change in reduced density matrix is quantified by the fidelity $F(\rho^{R'}, \rho^R)$ defined as

$$\sqrt{F(\rho^{R'}, \rho^R)} = \mathrm{tr}\sqrt{\sqrt{\rho^R}\rho^{R'}\sqrt{\rho^R}} = \mathrm{tr}(S), \quad (13)$$

where S is the diagonal matrix obtained from the singular value decomposition of $\sum_{\alpha,s_1} Y_t^{\alpha,s_1\dagger} Y_0^{\alpha,s_1} = USV^\dagger$. We define a threshold such that if the fidelity is less than that threshold, then the tensor closest to the boundary has changed sufficiently that the window needs to be expanded or moved to keep track of the wave front.

IV. NUMERICAL CALCULATIONS

In this section, we present numerical calculations for two dynamical window schemes: an *expanding window* in which the size of the window is grown to encompass the symmetrically expanding wave fronts, and a *moving window* in which the dynamical window is chosen to be much smaller to test the case that one is interested mainly in the dynamics of a small section of a larger system. In the latter case, a significant amount of the dynamics will occur outside of the window, so an important test of the method is to check that the dynamics within the window remains accurately described. For these calculations, we use the spin-1 AFM Heisenberg model represented by the Hamiltonian

$$H = \sum_i \vec{S}_i \cdot \vec{S}_{i+1} \quad (14)$$

subjected to a local perturbation S_0^+ applied at time $t = 0$ to the ground state $|\psi\rangle$, which we denote $|\Phi\rangle = S_0^+|\psi\rangle$. We compute some expectation values during the time evolution to compare with the fixed window method. Specifically, we are interested in observables such as local magnetization $\langle\Phi|S_x^z(t)|\Phi\rangle$ (x is the position of the lattice site) and the unequal time two-point correlator $A(x,t)$ given by

$$A(x,t) = \langle\psi|S_x^-(t)S_0^+(0)|\psi\rangle = \langle\psi|S_x^-(t)|\Phi\rangle. \quad (15)$$

From the unequal time two-point correlator one can extract the spectral function easily by employing the Fourier transform as follows:

$$S(q,\omega) = -\frac{1}{\pi}\mathrm{Im}\int_{-\infty}^{\infty} dt e^{i\omega t}\sum_x e^{-iqx} G(x,t), \quad (16)$$

where $G(x,t) = -iA(x,t)$ is the Green's function.

In our simulation, before applying the dynamical window techniques, we obtain the ground state of the infinite chain using the iTEBD algorithm.[24] This ground state is represented by a two-site translationally invariant MPS. By applying the IBC we represent the system with a finite-size MPS $|\psi\rangle$ to represent its ground state. Before evolving the system in time, we choose one site in the middle of the chain as the origin ($x = 0$) and perturb it by applying the spin-flip operator S^+ on the state $|\psi\rangle$ to obtain the excited state $|\Phi(t = 0)\rangle$. Note that when expanding or contracting the window, the number of sites added to or contracted from the window has to be a multiple of the unit cell, and here the unit cell contains two sites. Henceforth, a unit cell refers to two sites in this paper. We have implemented the TEBD with a fourth-order

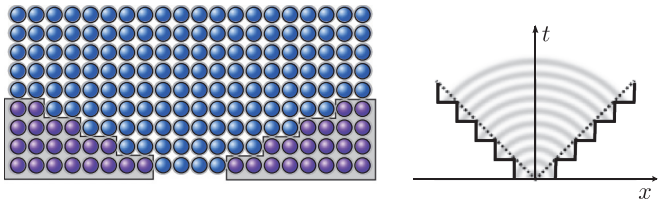

FIG. 3. (Color online) Illustration of how the window is expanded in time and space. The balls represent the lattice sites in the left figure: blue and purple balls are inside and outside the window, respectively. The black dotted lines in the right figure illustrate the wave front which propagates in time and space inside the window. The window is expanded both sides symmetrically as soon as the wave fronts hit the boundaries.

Suzuki-Trotter decomposition[25] with time step $\delta t = 0.05$ and keeping the number of states $\chi = 200$.

A. Expanding window

We start the time evolution of the system with a small window size N_e in which the perturbation appears in the middle at position $N_e/2$ sites in from the left boundary of the window. The expanding window scheme is illustrated in Fig. 3. When the wave fronts hit the boundaries, the window moving criterion describe in Sec. III C above is met, and we need to extend the window by adding some number of unit cells to both sides of the window. Here we add one unit cell at a time, however, in principle we can add an arbitrary number of unit cells in a single expansion step. After adding the sites, we evolve the system with the new window for some time before the next expansion procedure is initiated.

Figure 4 shows our numerical calculation of $\langle S^z(x,t)\rangle$. It also shows the result calculated with a fixed window of size $N_f = 240$ for comparison (this is numerically exact for these purposes). It can be seen that the results obtained from the different methods are almost the same, although the size of the starting window in the expanding case is much smaller $N_e = 8$ and increases slowly in time. Nevertheless, the expanding window calculation is much faster as the computation time is essentially linear in the size of the window.

In order to see how different are the wave packets between the expanding and fixed window methods, we plot the local magnetization $\langle S^z(x_j,t)\rangle$ at different positions x_j. The results are shown in Fig. 5 for $x_j = \{0,10,20,29\}$. We can see that they match very well. To see the differences in detail, we also plot absolute differences of $\langle S^z(x_j,t)\rangle$ between these two methods in Fig. 6(a). Note that, although both methods are implemented with the same time step, the Hamiltonian is treated differently inside and outside the window, which means that the Suzuki-Trotter error arising from the decomposition is slightly different in the two methods, although it is of the same magnitude. These differences saturate at an acceptably small value $\approx 10^{-4}$ which is comparable to the Suzuki-Trotter error. The threshold chosen for the fidelity also affects the accuracy. It is clear that the larger the threshold we keep, the longer time we evolve the system before expanding the window. However, if the threshold is too big, then the wave front will move ahead of the window and the calculation will lose accuracy. This is

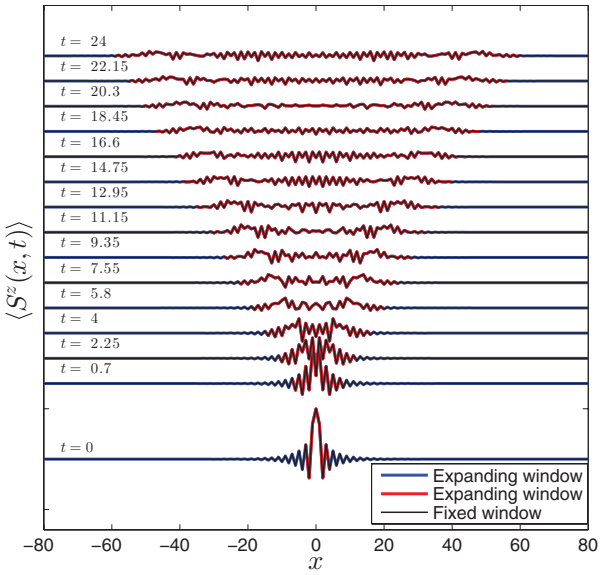

FIG. 4. (Color online) Comparison of a wave packet propagating in time between different schemes: fixed and expanding window. The red and blue lines represent the local magnetization $\langle S^z(x,t)\rangle$ inside and outside the window obtained from the expanding window technique, respectively. The label on each line corresponds to the time when the window is expanded by additional unit cells. The initial window size is $N_e = 8$, and two unit cells are added at each window edge to expand the window. The threshold $1 - \sqrt{F} = 10^{-3}$ is chosen for expanding the window criterion.

shown in Fig. 6(b), where we used the threshold 0.1, which is clearly leading to a loss of accuracy.

We also have tested that the expanding window technique can reproduce the spectral function of the system very well and is comparable with the result obtained from the fixed window technique. By Fourier transforming both in time and space the

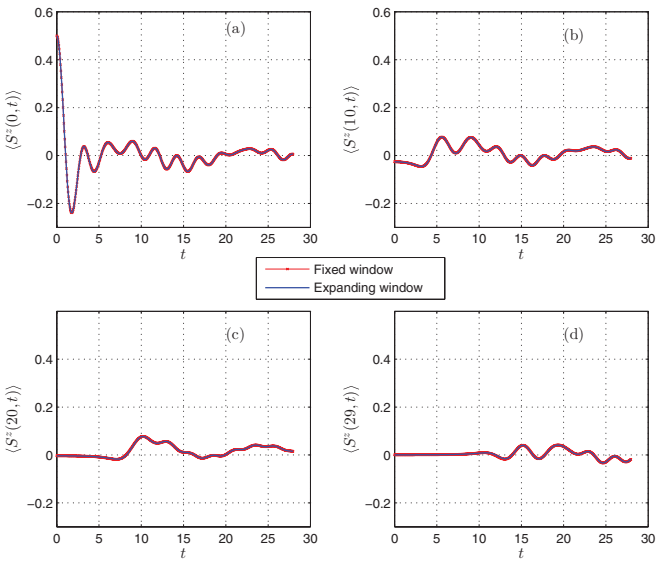

FIG. 5. (Color online) Comparison of local magnetization at specific positions x_j using two different schemes, the fixed window (red line) and expanding window (blue line). (a) $x_j = 0$; (b) $x_j = 10$; (c) $x_j = 20$; (d) $x_j = 29$.

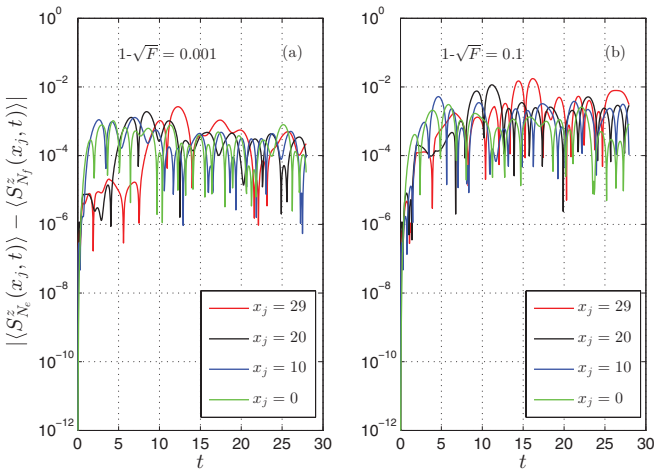

FIG. 6. (Color online) Absolute difference in local magnetization at positions x_j between the fixed and expanding window schemes. (a) Threshold $1-\sqrt{F}=0.001$. (b) Threshold $1-\sqrt{F}=0.1$.

Green's function $G(x,t)$ using Eqs. (15) and (16), we can get a full spectrum of the system. Figure 7(a) shows the spectral function of the system projected onto the plane of frequency ω and momentum q. We can extract the dispersion relation from it, which is plotted in Fig. 7(b) to compare with the result obtained from the fixed window technique. The plot shows that results obtained from the different methods are almost indistinguishable. In addition, the absolute difference of the Haldane gap computed by the two techniques is approximately equal to 10^{-4}.

B. Moving window

In the dynamical window technique it is possible to combine both the expansion and contraction steps. The window is now fixed in size and is shifted along the chain as soon as the wave fronts hit the boundary. In principle, we can move this window to either side of the chain. In Fig. 8, the initial window contains $N=4$ sites and starts moving from the right to the left of the spin chain (the positive direction is chosen to the left). As a result of moving the window, the wave front will cross over the right boundary, but on the left side the wave front will not propagate through the boundary. Therefore, all the dynamical properties measured in the region colored blue and purple should be reliable, but not for the black region, as the wave function there is represented only by the boundary tensor and hence is restricted to a χ-dimensional effective Hilbert space.

The advantage of this scheme is that it is very cheap in computational cost as we just need to modify and update the sites inside the window, which can be kept as small as possible. To understand how it is implemented in terms of a tensor network, we introduce the update scheme for MPS and effective Hamiltonian before the window is shifted to a new position. They are the two most important components in the update scheme of the real-time evolution algorithm of the MPS with IBC.

The procedure for updating the new window is described in Fig. 9, where a unit cell is added or removed from the window. When the moving window criterion is met, we need to shift the window to the left by one unit cell. Note that

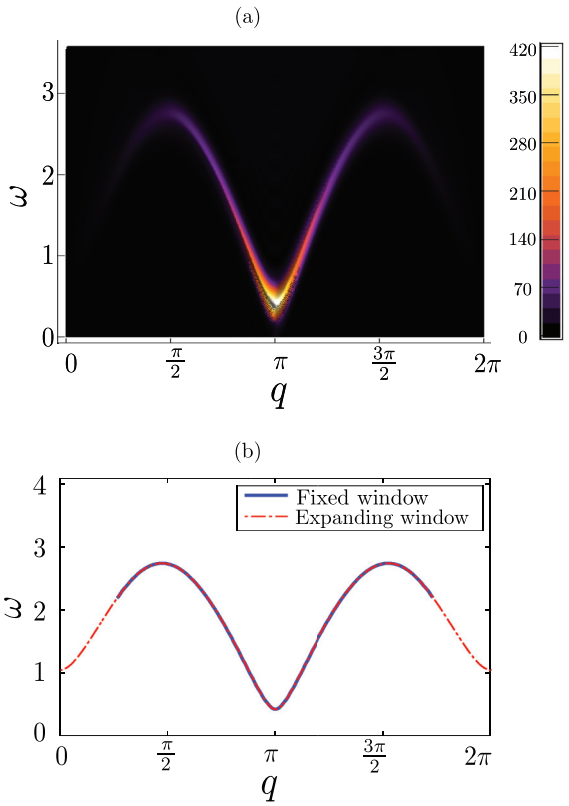

FIG. 7. (Color online) (a) The spectrum obtained from the expanding window technique is projected onto the plane of frequency ω and momentum q. (b) Comparison of the dispersion relations between the fixed and expanding window techniques with window sizes $N_f=60$ and $N_e=8$, respectively. The Haldane gap is $\Delta_f \approx 0.4105$ for the fixed window and is $\Delta_e \approx 0.4104$ for the expanding window.

the number of sites in the old window that are absorbed into the right boundary is equal to the number of sites added to the left edge of the window to keep the overall size of the window constant. However, it is possible to arbitrarily enlarge or contract the window throughout the calculation, in cases where that is desirable.

In addition to updating the MPS tensors for the wave function inside the window, we need to update the effective Hamiltonian. In fact, as the window is translated to the left, because the tensors that represent the semi-infinite strip to

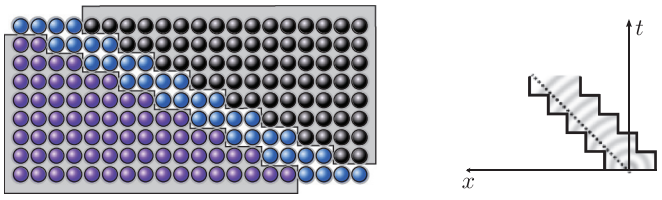

FIG. 8. (Color online) Illustration of how the window is translated in time and space. The balls represent the lattice sites in the left figure: Blue balls are inside the window; purple and black balls are outside on the left and the right of the window, respectively. The black dotted lines in the right figure show the wave front propagating in time and space inside the window. The window moves along the spin chain axis as soon as the wave fronts hit the left boundary.

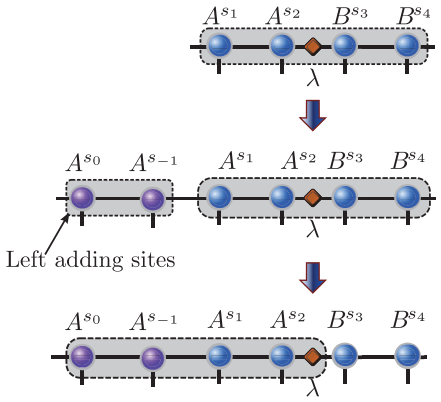

FIG. 9. (Color online) Illustration of how to update the MPS when moving the window to the left. One unit cell is added to the left edge of the old window while a unit cell on the right edge of the old window is absorbed into the right boundary tensor.

the left are translationally invariant, the effective Hamiltonian and left block operators remain unchanged, while the right effective Hamiltonian and block operators must be updated to incorporate the changed sites of the window that are now incorporated into the right boundary. This is done via Eq. (11) with the graphical illustration in Fig. 2 to update the components of the effective Hamiltonian and block operators.

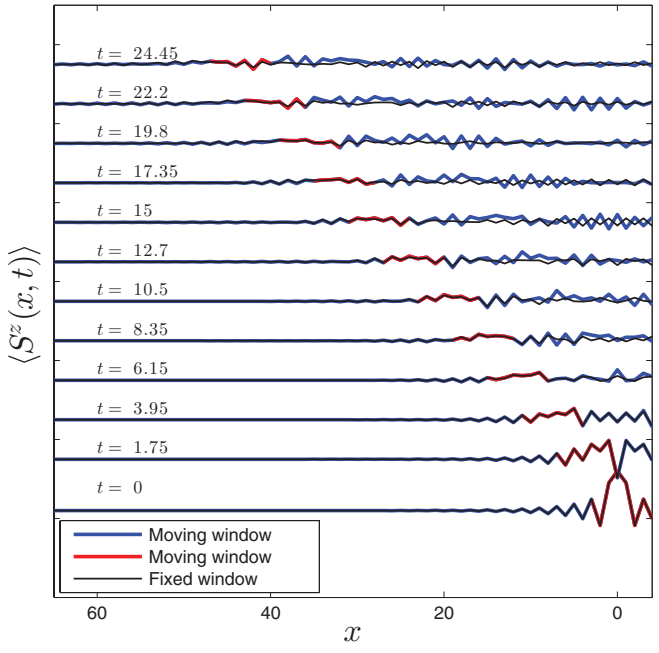

FIG. 10. (Color online) Comparison of the wave packet propagating in time for the fixed and moving window schemes. The black lines correspond to the fixed window with size $N_f = 240$. The red and blue lines correspond to the cases of inside and outside of the moving window with size $N_m = 8$, respectively. The time labeled on each line corresponds to the time when the window is translated to the left side of the chain. Two unit cells are added to the left window edge and four sites on the right of the window are contracted to the right boundary to keep the window size unchanged. The threshold $1 - \sqrt{F} = 0.005$ was chosen for the moving window criterion.

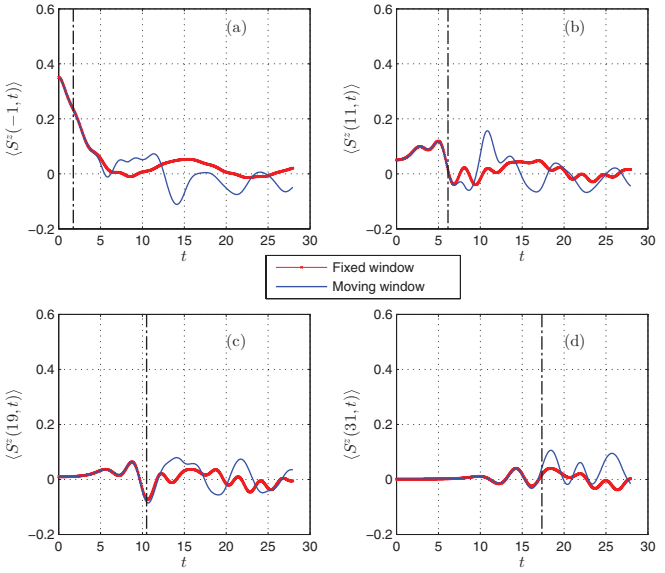

FIG. 11. (Color online) Comparison of local magnetization evolving in time at specific positions x_j on the left side of the perturbation point between the different schemes: fixed and moving window. The size of the fixed window is $N_f = 240$ and $N_m = 8$ for the moving window. (a) $x_j = -1$; (b) $x_j = 11$; (c) $x_j = 19$; (d) $x_j = 31$. The dashed-dotted vertical line in each subplot points out the time when the corresponding site at that position is out of the window and absorbed into the right boundary.

Again, we study the local magnetization $\langle S^z(x,t)\rangle$ and compare with the result obtained for the fixed window case. The comparison is plotted in Fig. 10. In our numerical calculation the size of the moving window is chosen to be $N_m = 8$, compared to the size of a fixed window $N_f = 240$. We can see that the moving window captures well the wave front propagating to the left, and in this region it compares well with the results from the fixed window. Once the moving window has passed by, corresponding to the black region in Fig. 8, the deviation is quite large because these sites have been absorbed into the right boundary and are therefore represented only in a small χ-dimensional Hilbert space. However, if we are interested primarily in the state of the system in the vicinity of the wave front, then the moving dynamical technique is a great advantage as the costly time evolution procedure is only carried out on a very small number of tensors. Thus this approach can be an order of magnitude more efficient than the fixed or expanding window approach.

We now examine the local magnetizations at some specific positions of the spin chain. In Fig. 11, we plot $\langle S^z(x_j,t)\rangle$ at $x_j = \{-1,11,19,31\}$. We can see that in all four subplots $\langle S^z(x_j,t)\rangle$ calculated using the moving window is quite similar to that of the fixed window when the site is inside or to the left of the window. Specifically, the further away from the initial perturbation point, the longer is the time scale for which we can obtain accurate results. This is easy to understand as it takes a longer time for the window to move to the further sites of the chain, and the region to the left of the chain is well described by the Hilbert space of the semi-infinite chain. When the window passes by a region of the lattice, these sites are absorbed into the right boundary, so this causes the results

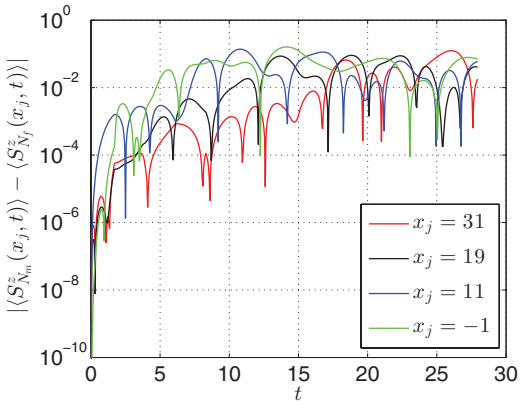

FIG. 12. (Color online) Difference in local magnetizations evolving in time at specific positions x_j on the left side of the perturbation point between the different schemes: fixed and moving window.

measured after that time to be less accurate. Hence we see a large deviation in the results at a time that corresponds to the moving window having passed by the measurement location.

For a clearer comparison of $\langle S^z(x_j,t)\rangle$, we also plot the absolute difference between the two schemes in Fig. 12. We can see that at the early time the differences seem to be small and then increase in time. These errors can be well controlled by manipulating the size of the window and the criteria for moving the window.

The moving window technique is not so appropriate for calculating the spectral function, since to obtain an accurate real-space Fourier transform we need accurate data over a large section of the lattice. However, the moving window technique comes into its own for examining the dynamics of the wave front itself, for example, even a small moving window calculation should be adequate for distinguishing ballistic versus diffusive transport. However, for the purpose of comparison with the other techniques of fixed and expanding window, we can also calculate the spectral function by increasing the size of the window and exploiting the reflection symmetry of the system. In Fig. 13(a), we show the plot for the spectral function projected onto the frequency and momentum plane. The window size in this case is chosen as $N_m = 40$. Note that in order to obtain the spectral function, one needs to calculate the unequal time two-point correlator $A(x,t)$. Thanks to the reflection symmetry of the system, $A(-x,t) = A(x,t)$, we only need to compute this quantity for positive x. Then whenever the middle site of the initial window (the perturbed site) is still inside the window, we can obtain a reliable result for $A(x,t)$ ($x \geqslant 0$). We also plot the comparison of dispersion relations between two schemes in Fig. 13(a) and it seems to fit very well. The absolute difference of the Haldane gap obtained is of order 10^{-2}. This difference can be reduced by increasing the size of the window, trading off increased computation.

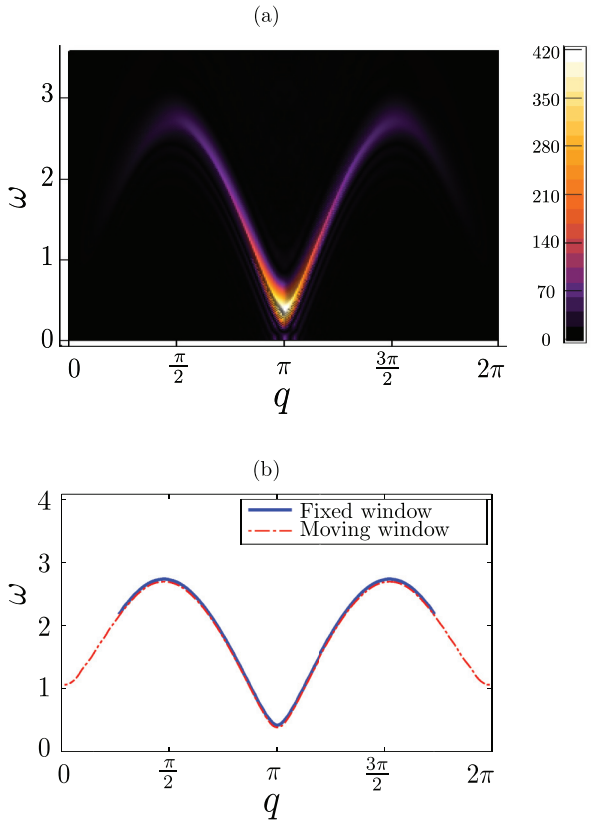

FIG. 13. (Color online) (a) The spectrum obtained from the moving window technique is projected onto the plane of frequency ω and momentum q. (b) Comparison of the dispersion relations between the fixed and moving window techniques with window sizes $N_f = 60$ and $N_m = 40$, respectively.

V. CONCLUSION

We have introduced two dynamical window techniques for studying the real-time evolution of a locally perturbed infinite 1D system, the expanding window and the moving window. Taking advantage of infinite boundary conditions, which have been introduced to replace an infinite MPS by a finite MPS, we have proved that these two techniques are viable and are a more efficient replacement for the fixed window technique.

One of the great advantages of these techniques is a large savings in computational resources as we only need to compute the evolution of a small window of the system. This is most significant for the moving window technique, where the computational cost per time step does not increase as the perturbation propagates through the system. This is particularly relevant for cases where the region of interest is quite small, for example, the immediate vicinity of the wave front. For calculating quantities such as the spectral function, we are interested in regions only where the correlation function differs significantly from zero, so this approach, where the dynamics are obtained accurately in a small region and approximated elsewhere, is a significant improvement.

In these techniques, the choice of window size is critical. We have introduced a criterion for automatically adjusting the window, utilizing a fidelity threshold $1 - \sqrt{F}$. This can be tuned such that the window tracks the wave front, however, if the value is chosen inappropriately, the calculation will be inaccurate or inefficient. For instance, in the expanding window technique, the sharper the threshold, the more accurate is the result we obtain. However, this may lead to a fast growing window size and therefore may limit the efficiency

(however, it will still be more efficient than a large fixed window). In the moving window technique, if the threshold is chosen to be either too large or too small, then there is a danger that the wave front will move out of the window, which will cause a severe loss of accuracy. However, there seems to be a fairly large range of thresholds which successfully capture the wave front in a near-optimal fashion so, in practice, choosing an appropriate threshold appears to be not so difficult.

Note added. Recently we learned of some related works.[26,27]

ACKNOWLEDGMENT

We acknowledge support from the Australian Research Council Centre of Excellence for Engineered Quantum Systems and the Discovery Projects funding scheme (Project No. DP1092513).

[1] S. R. White, Phys. Rev. Lett. **69**, 2863 (1992).
[2] S. R. White, Phys. Rev. B **48**, 10345 (1993).
[3] K. A. Hallberg, Phys. Rev. B **52**, R9827 (1995).
[4] T. D. Kühner and S. R. White, Phys. Rev. B **60**, 335 (1999).
[5] E. Jeckelmann, Phys. Rev. B **66**, 045114 (2002).
[6] M. A. Cazalilla and J. B. Marston, Phys. Rev. Lett. **88**, 256403 (2002).
[7] X. Wang and T. Xiang, Phys. Rev. B **56**, 5061 (1997).
[8] J. Sirker and A. Klumper, Phys. Rev. B **71**, 241101 (2005).
[9] S. Ostlund and S. Rommer, Phys. Rev. Lett. **75**, 3537 (1995).
[10] M. Fannes, B. Nachtergaele, and R. Werner, Commun. Math. Phys. **144**, 443 (1992).
[11] D. Perez-Garcia, F. Verstraete, M. M. Wolf, and J. I. Cirac, Quantum Inf. Comput. **7**, 401 (2007).
[12] G. Vidal, Phys. Rev. Lett. **91**, 147902 (2003).
[13] G. Vidal, Phys. Rev. Lett. **93**, 040502 (2004).
[14] S. R. White and A. E. Feiguin, Phys. Rev. Lett. **93**, 076401 (2004).
[15] A. J. Daley, C. Kollath, U. Schollwoeck, and G. Vidal, J. Stat. Mech.: Theor. Exp. (2004) P04005.
[16] J. Haegeman, J. I. Cirac, T. J. Osborne, I. Pižorn, H. Verschelde, and F. Verstraete, Phys. Rev. Lett. **107**, 070601 (2011).
[17] J. Haegeman, B. Pirvu, D. J. Weir, J. I. Cirac, T. J. Osborne, H. Verschelde, and F. Verstraete, Phys. Rev. B **85**, 100408(R) (2012).
[18] A. E. Feiguin and S. R. White, Phys. Rev. B **72**, 020404 (2005).
[19] T. Enss and J. Sirker, New J. Phys. **14**, 023008 (2012).
[20] E. H. Lieb and D. W. Robinson, Commun. Math. Phys. **28**, 251 (1972).
[21] M. C. Bañuls, M. B. Hastings, F. Verstraete, and J. I. Cirac, Phys. Rev. Lett. **102**, 240603 (2009).
[22] H. N. Phien, G. Vidal, and I. P. McCulloch, Phys. Rev. B **86**, 245107 (2012).
[23] L. Michel and I. P. McCulloch, arXiv:1008.4667.
[24] G. Vidal, Phys. Rev. Lett. **98**, 070201 (2007).
[25] N. Hatano and M. Suzuki, in *Quantum Annealing and Other Optimization Methods*, edited by A. Das and B. K. Chakrabarti, Lecture Notes in Physics Vol. 679 (Springer, Berlin, 2005), pp. 37–68.
[26] V. Zauner, M. Ganahl, H. G. Everts, and T. Nishino, arXiv:1207.0862.
[27] A. Milsted, J. Haegeman, T. J. Osborne, and F. Verstraete, arXiv:1207.0691.